

BigStitcher: Efficient alignment of large multi-tile and multi-view image datasets

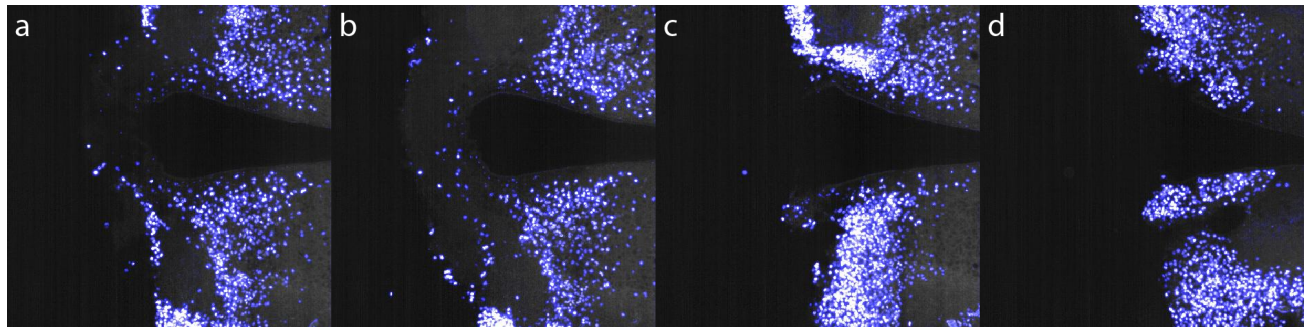
David Hörl, Fabio Rojas Rusak, Stephan Preibisch

Supplementary File	Title
Supplementary Figure 1	Fluorescence preservation in cleared samples
Supplementary Figure 2	Illumination selection
Supplementary Figure 3	Manual alignment
Supplementary Figure 4	Flat-field correction
Supplementary Figure 5	Pairwise registration by phase correlation
Supplementary Figure 6	Downsampling with different SNR
Supplementary Figure 7	Downsampling error statistics 1
Supplementary Figure 8	Downsampling error statistics 2
Supplementary Figure 10	Downsampling error statistics 3
Supplementary Figure 20	Interactive inspection and curation of pairwise links
Supplementary Figure 14	Global optimization
Supplementary Figure 15	Affine refinement via ICP
Supplementary Figure 16	Interest point visualization
Supplementary Figure 17	Manual Transformation of multi-view datasets
Supplementary Figure 18	Bounding Box definition
Supplementary Figure 19	Virtual fusion of large image
Supplementary Note 1	Supplementary methods
Supplementary Note 2	BigStitcher User Guide
Supplementary Note 3	Links to the current source codes

Note: Supplementary Videos 1–XXX are available for download on the journal homepage.

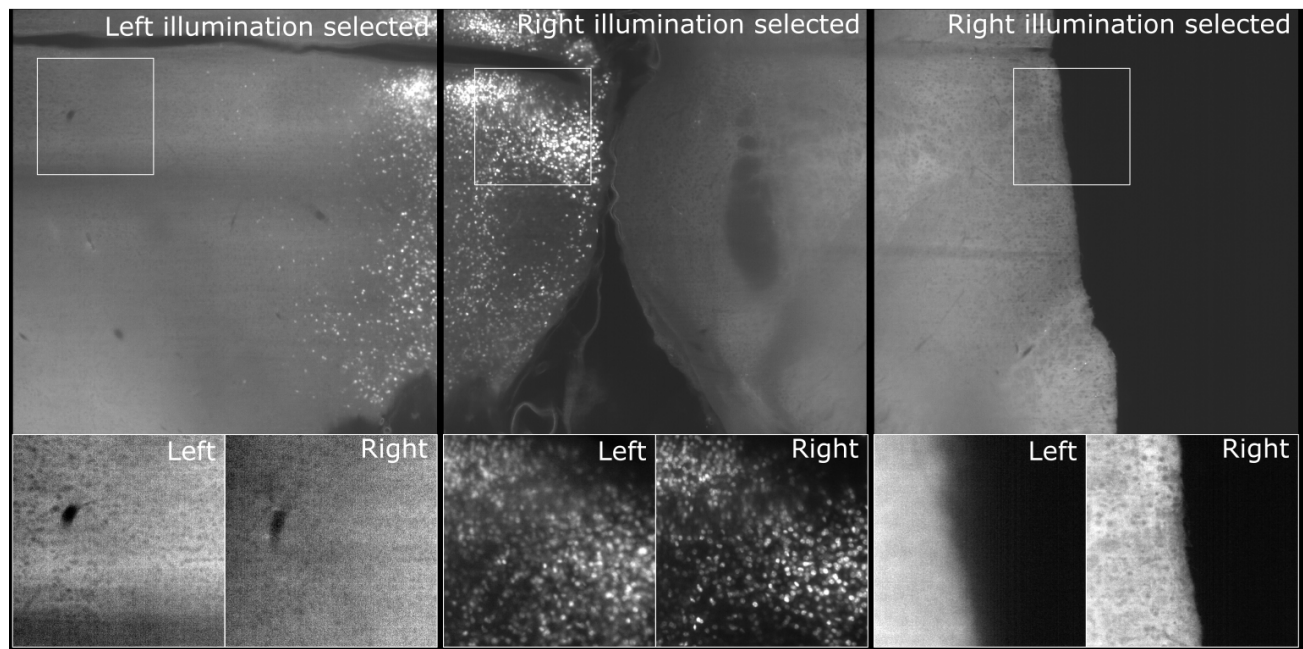
SUPPLEMENTARY FIGURES

SUPPLEMENTARY FIGURE 1: Fluorescence preservation in cleared samples



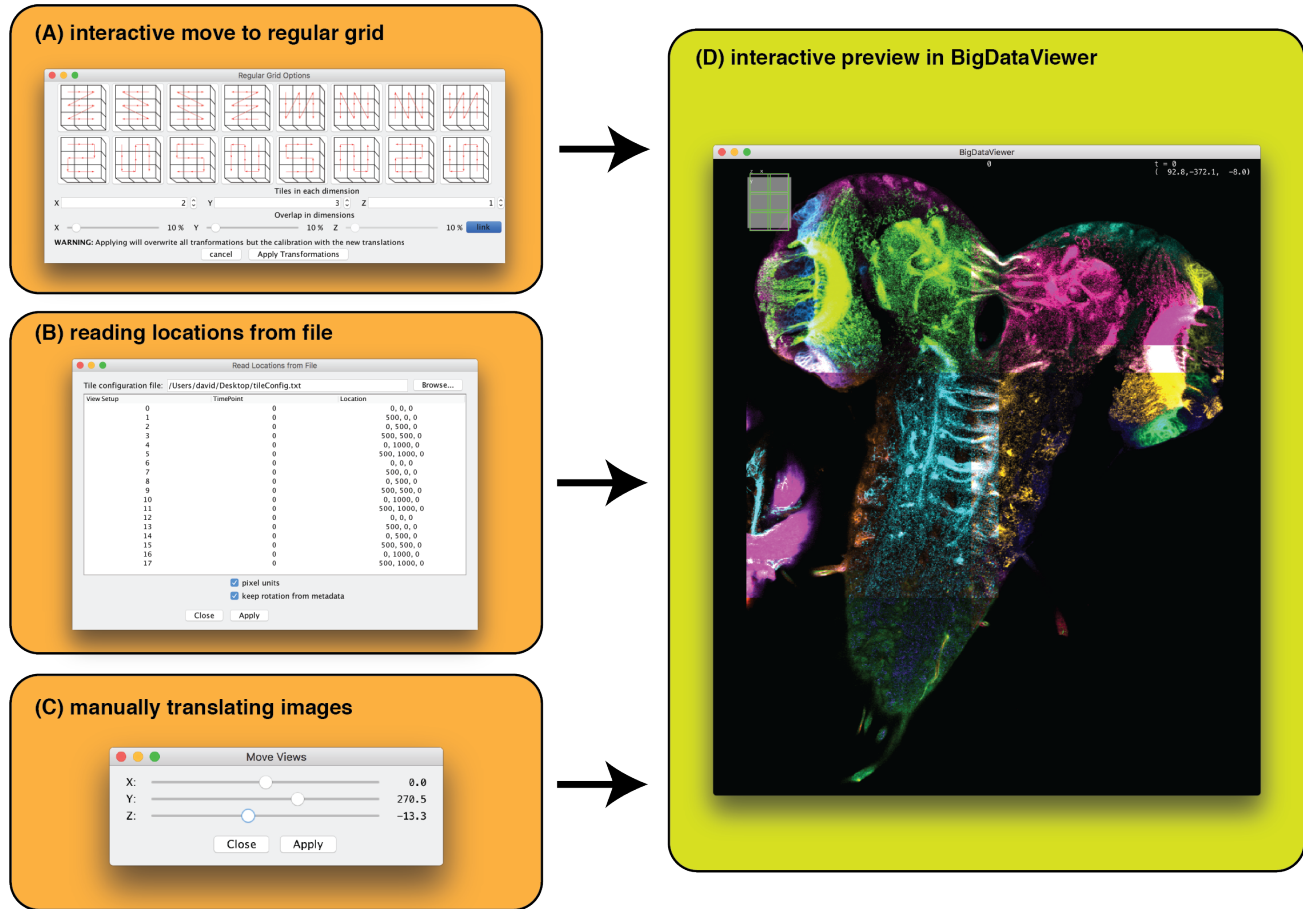
Supplementary Figure 1: *Fluorescence preservation and image analysis in cleared samples.* (a)-(d) Optical sections of (??structure??) in a CLARITY-cleared adult mouse brain expressing ??Histone-GFP?? in ??which cells??. Fluorescence is preserved throughout the clearing procedure and can be used in advanced image analyses. The examples show nuclear segmentation via pixel-wise classification by a Random Forest⁷ model. Classification results (probability maps) are overlaid in blue on the grayscale raw intensities.

SUPPLEMENTARY FIGURE 2: Illumination selection



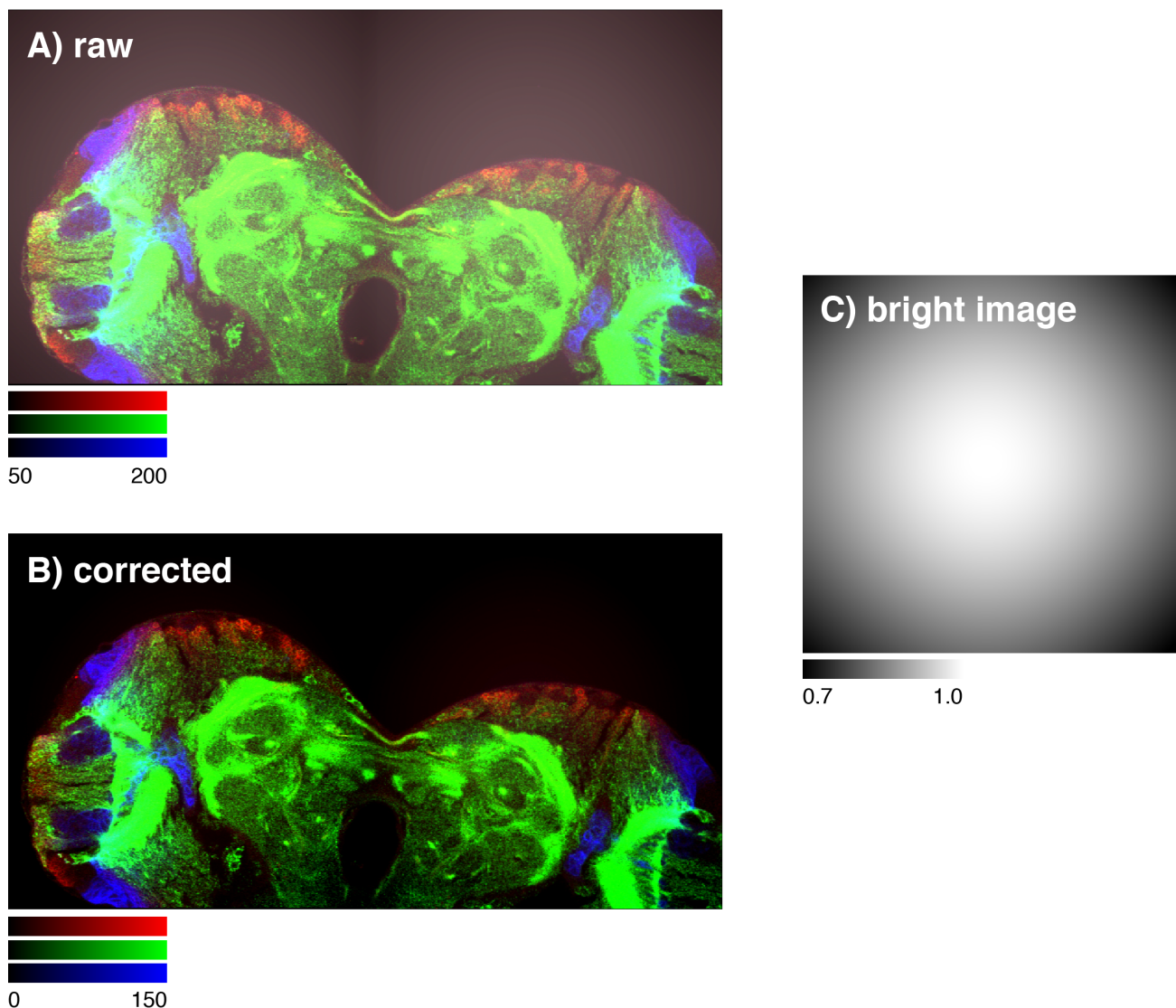
Supplementary Figure 2: *Automatic illumination selection*. Best illumination for three consecutive tiles was selected based on brightest view for each tile. Close-ups shows the specified region for both illumination directions.

SUPPLEMENTARY FIGURE 3: Manual alignment



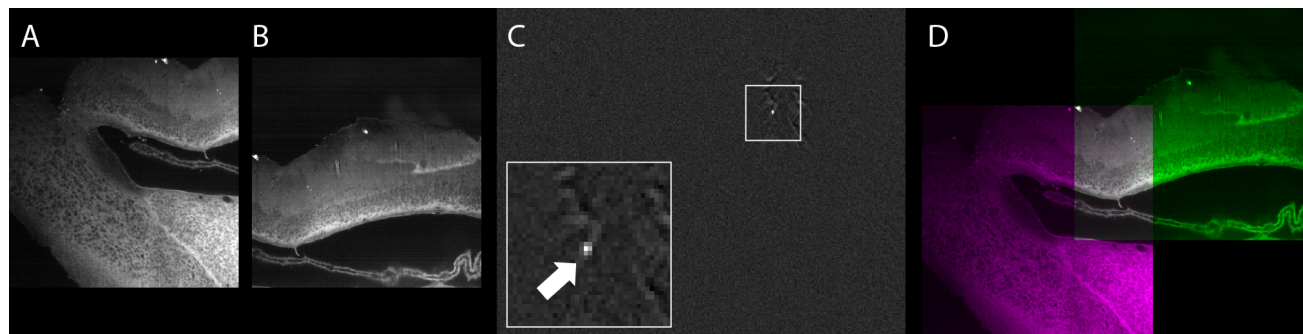
Supplementary Figure 3: *Interactive manual alignment of tiled images.* The BigStitcher GUI offers various ways of manually (pre-)aligning tiled images. Images can be moved to a regular grid with a given tile order and overlap (**A**). Image locations can also be read from a simple *tile configuration* text file (**B**). Furthermore, selected image(s) can be moved along axes via sliders (**C**). All changes will be displayed in the BigDataViewer window immediately (**D**) for quick verification.

SUPPLEMENTARY FIGURE 4: Flat-field correction



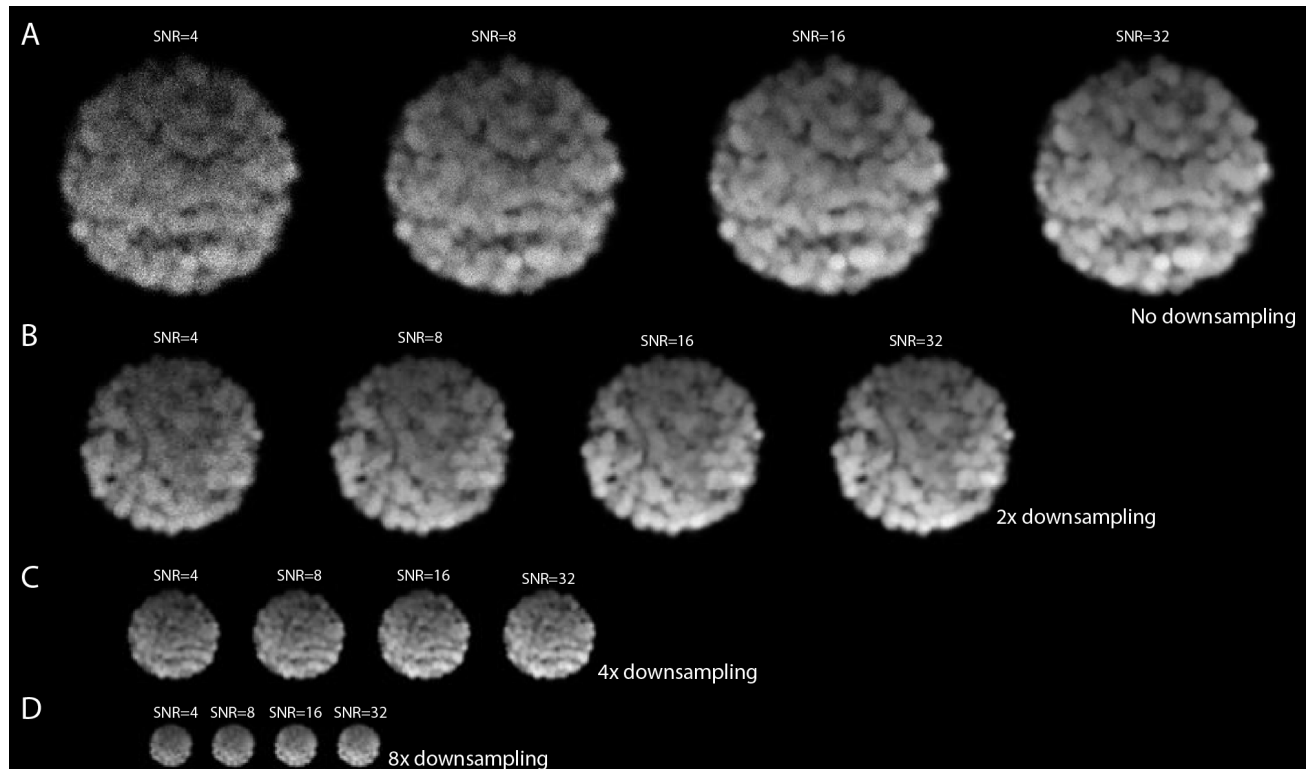
Supplementary Figure 4: *On-the-fly flat-field correction*. The BigStitcher offers correction for camera offsets, fixed pattern noise or uneven illumination. **(A)**: Simulation of the effects of a constant background offset and Gaussian illumination/detection efficiency **(C)** on tiled images. By subtracting the *dark image* and modulating with the inverse relative intensity of the *bright image*, such artefacts can be corrected easily **(B)**. The correction is calculated virtually, with optional cacheing, to allow for immediate inspection of the results.

SUPPLEMENTARY FIGURE 5: Pairwise registration by phase correlation



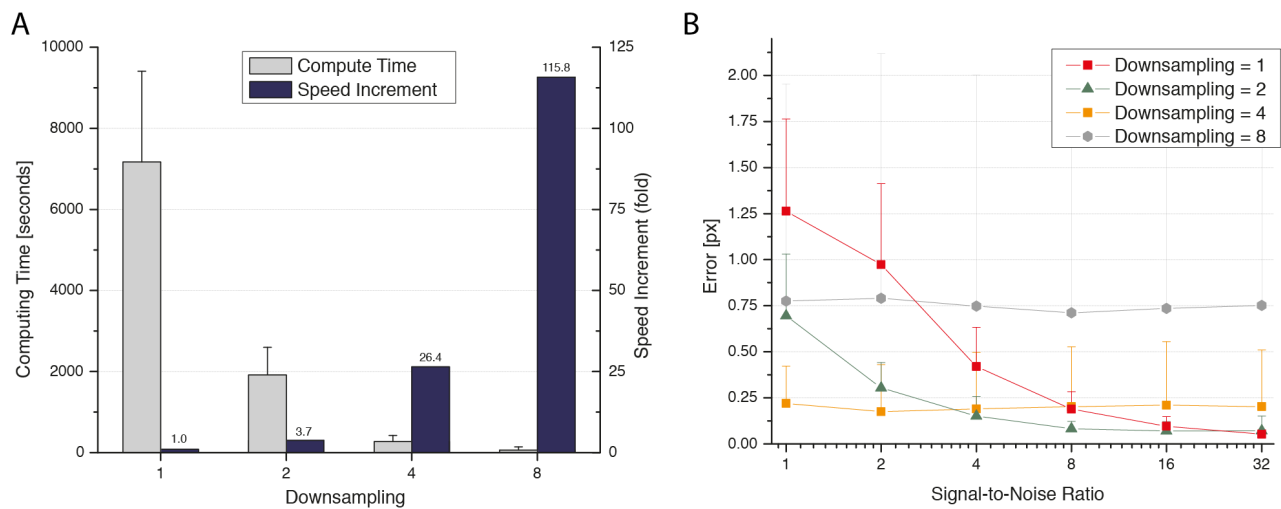
Supplementary Figure 5: *Pairwise registration by phase correlation.* (A),(B) Central slices of image stacks from a tiled acquisition (non-regular tiling) of an adult mouse hypothalamus slice. (C) Phase correlation matrix (PCM) calculated from the two images shows a single, distinct peak above nearly constant background. The peak location corresponds to the relative translation t of both tiles. (D) Central slice through the images aligned according to t , as displayed in BigDataViewer.

SUPPLEMENTARY FIGURE 6: Downsampling with different SNR



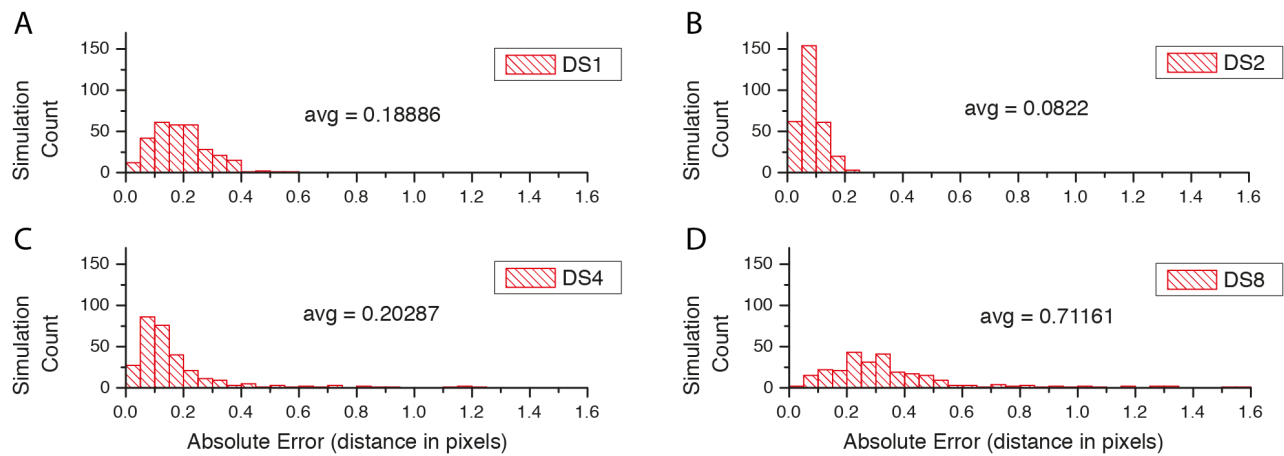
Supplementary Figure 6: *Effects of downsampling on simulated data with different SNR.* (A) Simulated image stacks of spheroid-like objects deteriorated by anisotropic sampling, light attenuation, convolution with an anisotropic PSF, and pixel intensity generation using Poisson processes to archive desired signal-to-noise-ratios (SNRs). (B), (C), (D) Effects of downsampling (with Gaussian smoothing for anti-aliasing) on the simulated images. The effects of Poissonian Shot noise are gradually reduced by the blurring of increasing downsampling.

SUPPLEMENTARY FIGURE 7: Downsampling statistics 0



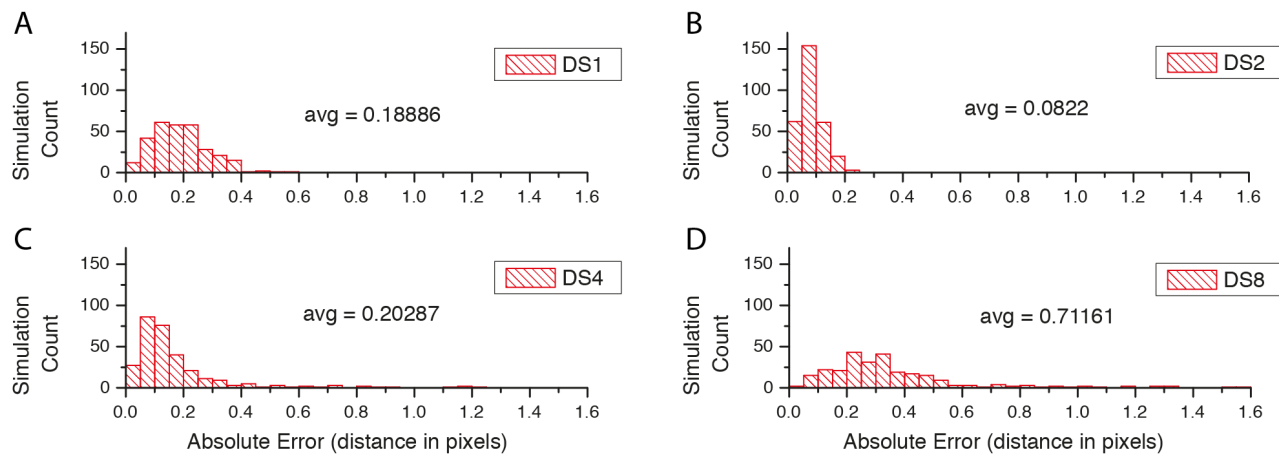
Supplementary Figure 7: *Lorem ipsum.* Dolor sit amet.

SUPPLEMENTARY FIGURE 7b: Downsampling statistics 1



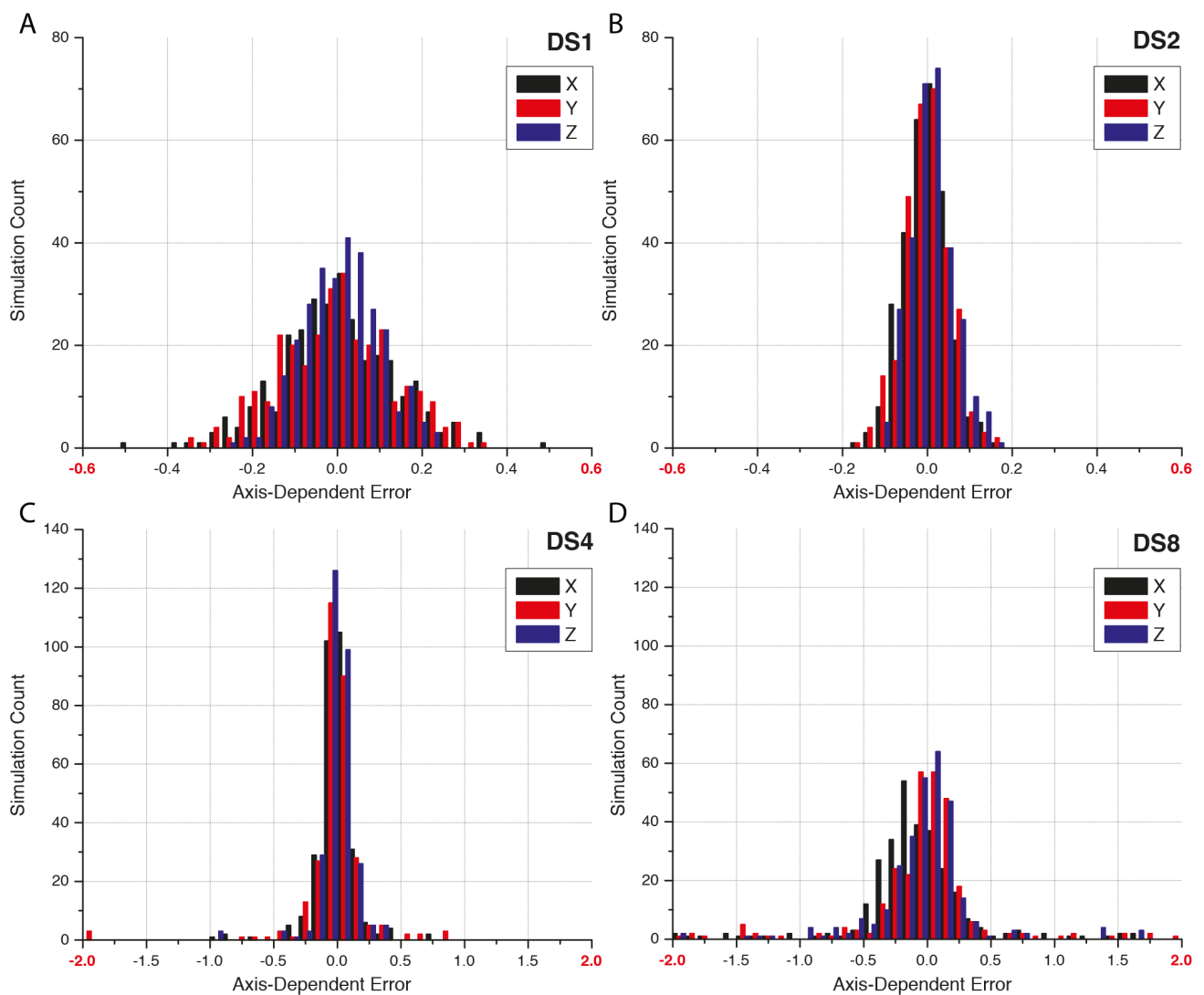
Supplementary Figure 8: *Lorem ipsum. Dolor sit amet.*

SUPPLEMENTARY FIGURE 8: Downsampling statistics 2



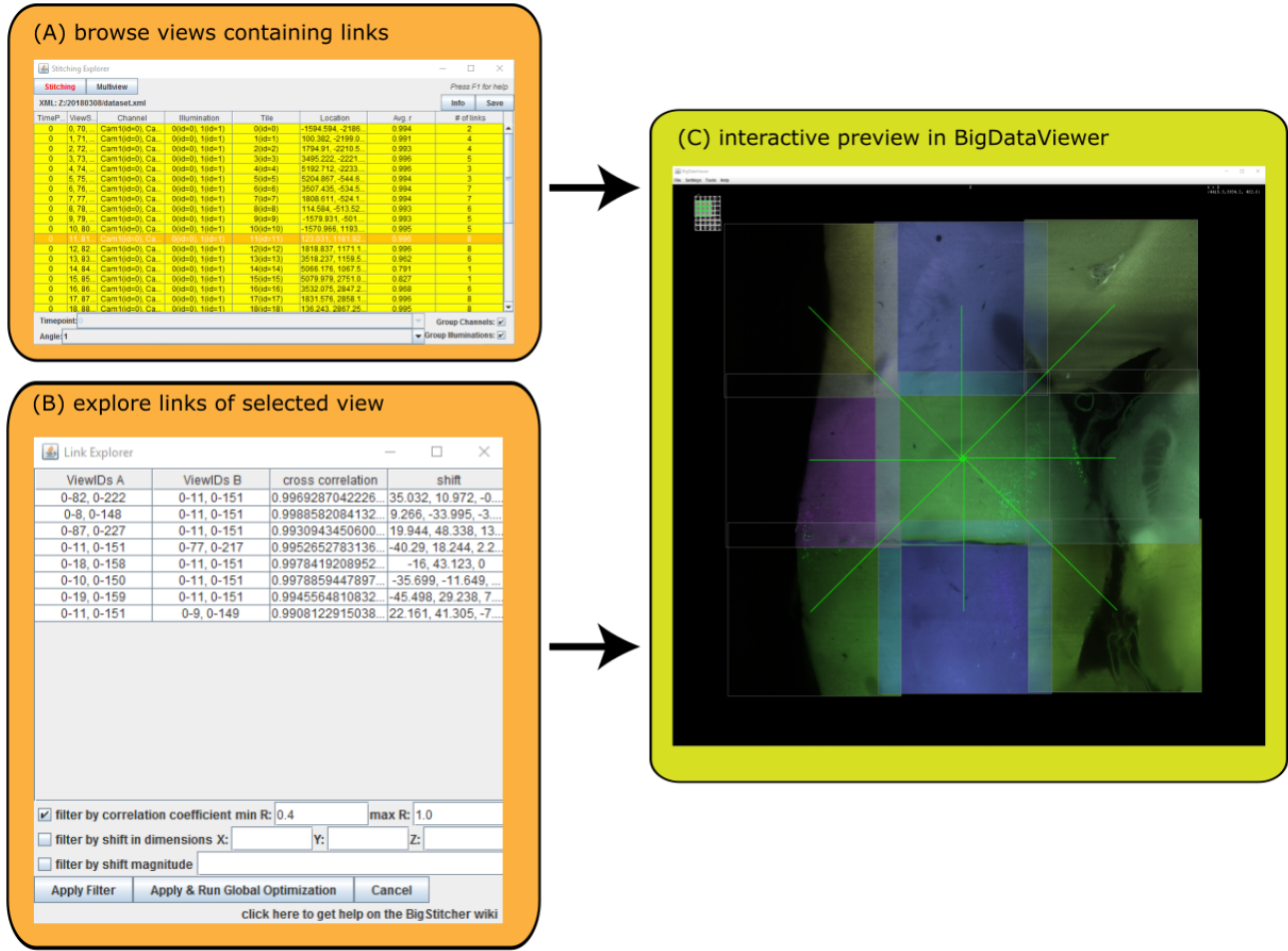
Supplementary Figure 9: *Lorem ipsum. Dolor sit amet.*

SUPPLEMENTARY FIGURE 9: Downsampling statistics 3



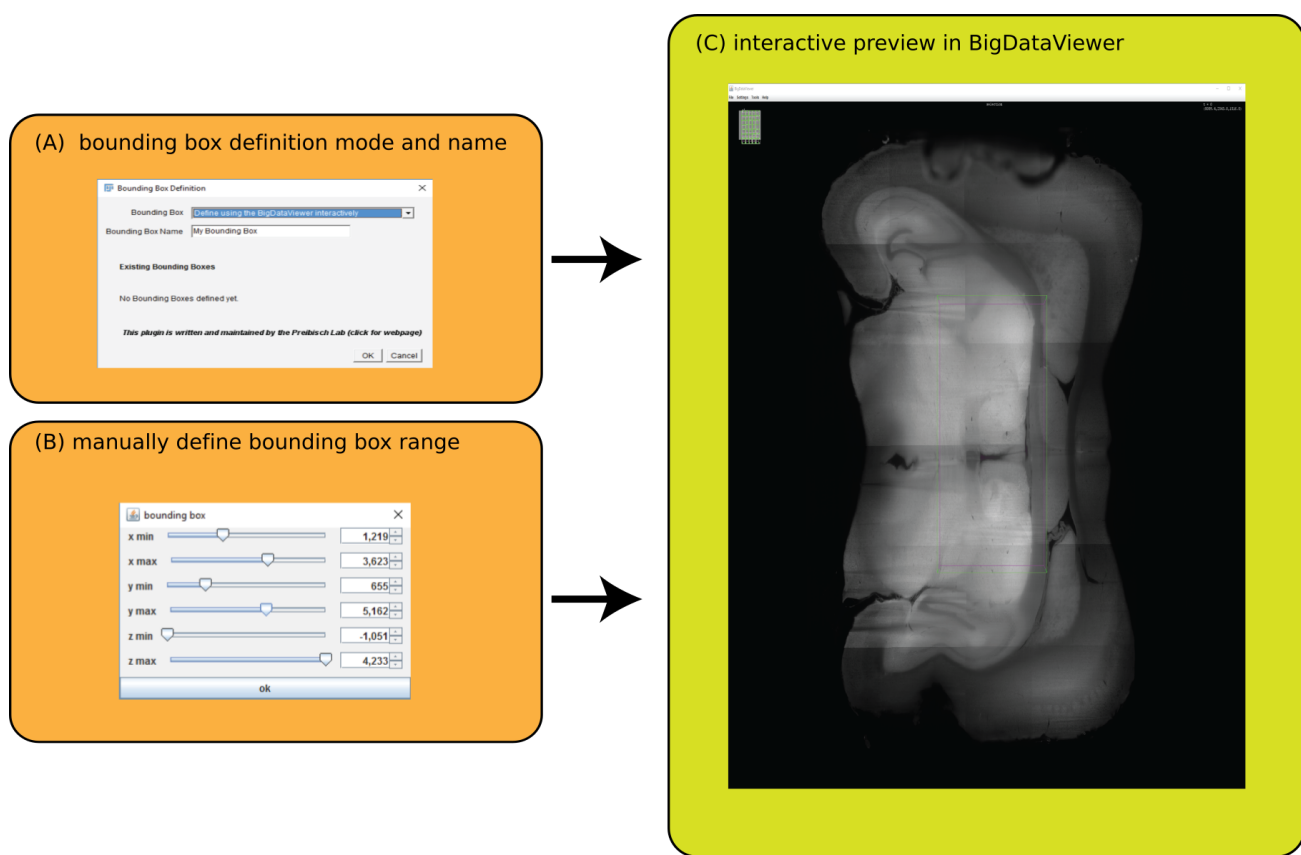
Supplementary Figure 10: *Lorem ipsum.* Dolor sit amet.

SUPPLEMENTARY FIGURE 10: Interactive inspection and curation of pairwise links



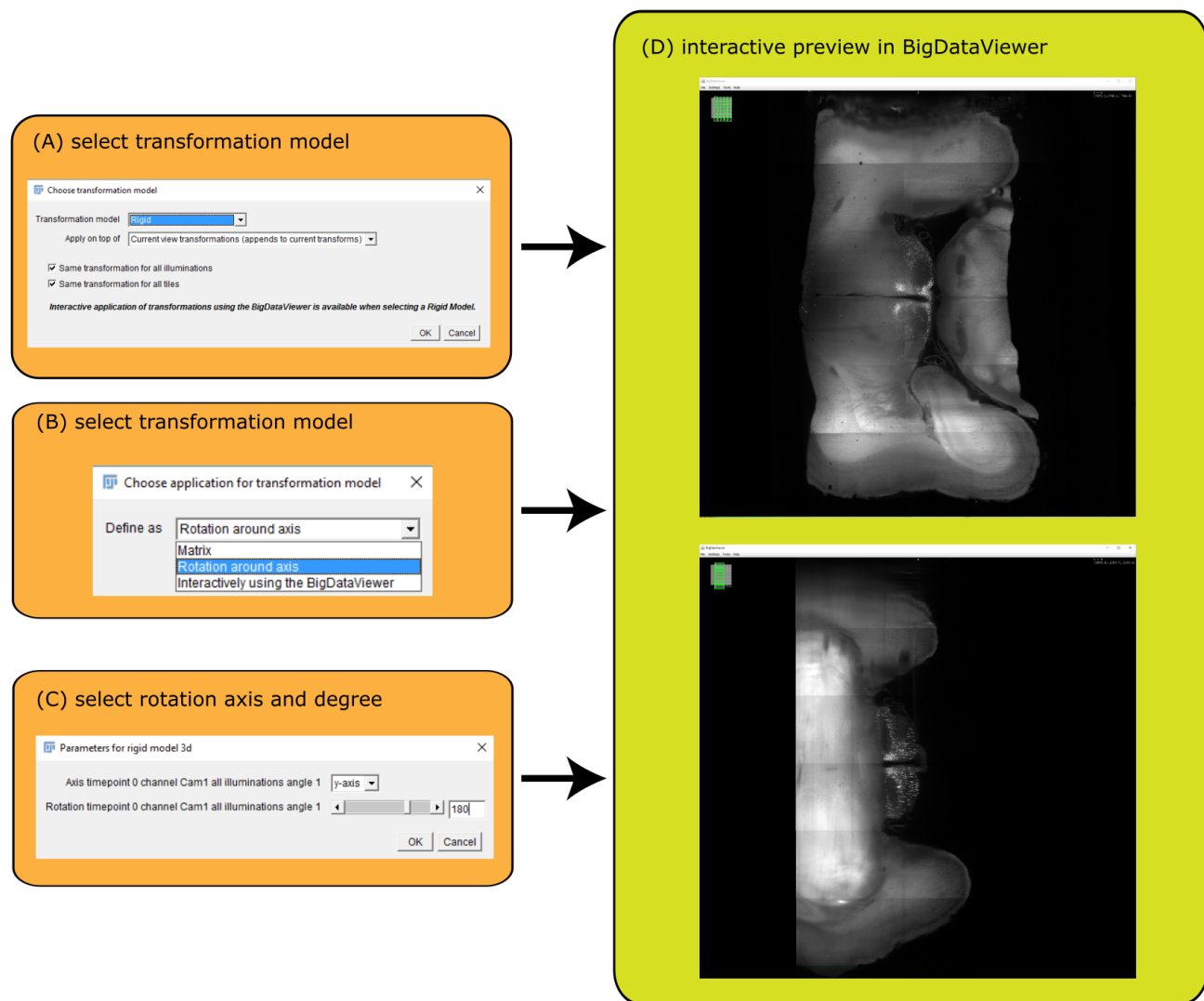
Supplementary Figure 11: *Interactive visualization of links in the link explorer*. The BigStitcher GUI offers the exploring and modifying calculated links between corresponding tiles in the link explorer menu. **(A)** Tiles containing links are displayed in yellow and can be selected. **(B)** Display corresponding tiles of the selected view. Single links can be removed manually or through available filtering options. **(C)** Corresponding links of the selected view are displayed in real-time in the BigDataViewer.

SUPPLEMENTARY FIGURE 10b: Bounding Boxes



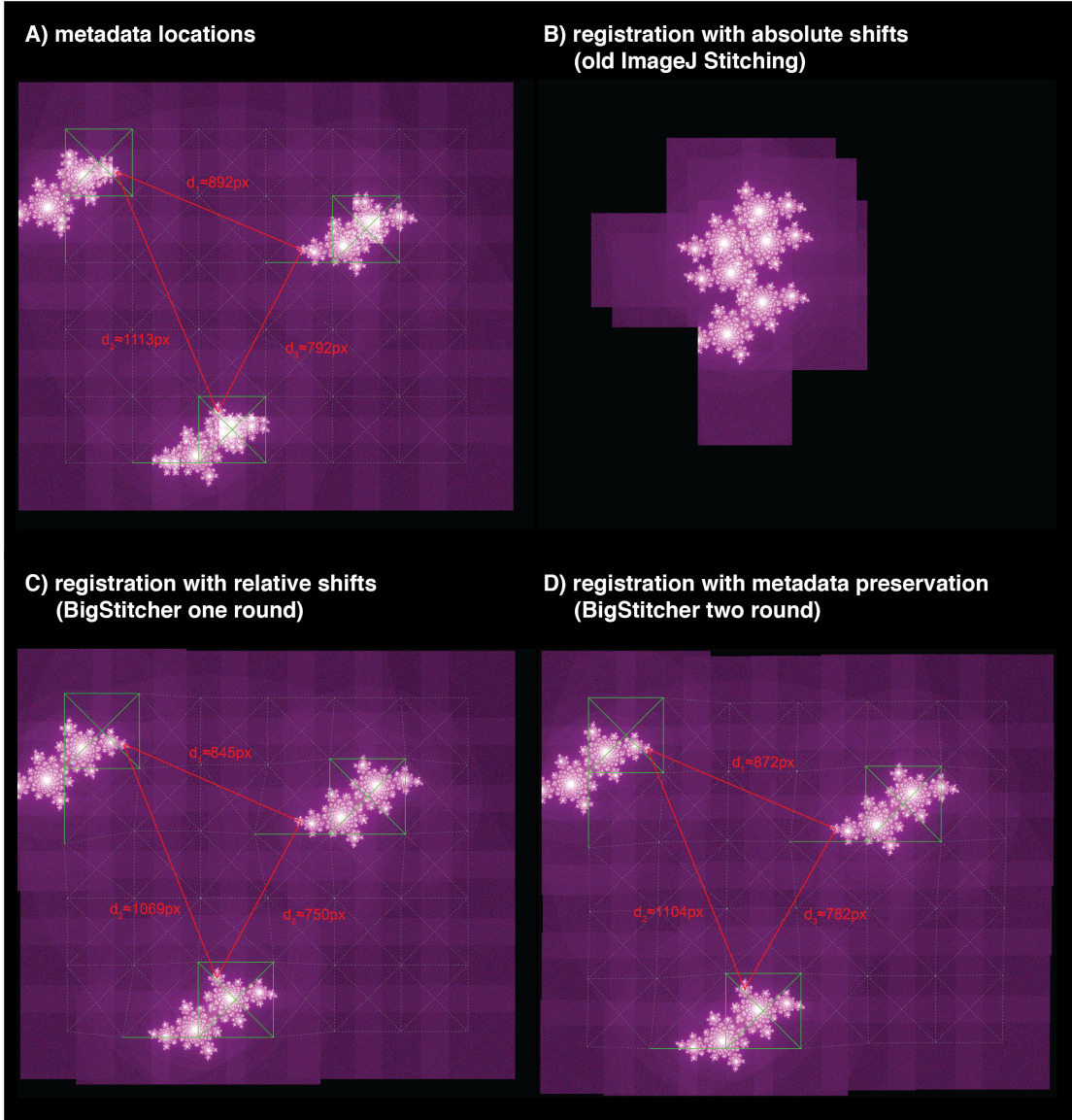
Supplementary Figure 12: *Lorem ipsum. Dolor sit amet.*

SUPPLEMENTARY FIGURE 10c: Apply Transformations



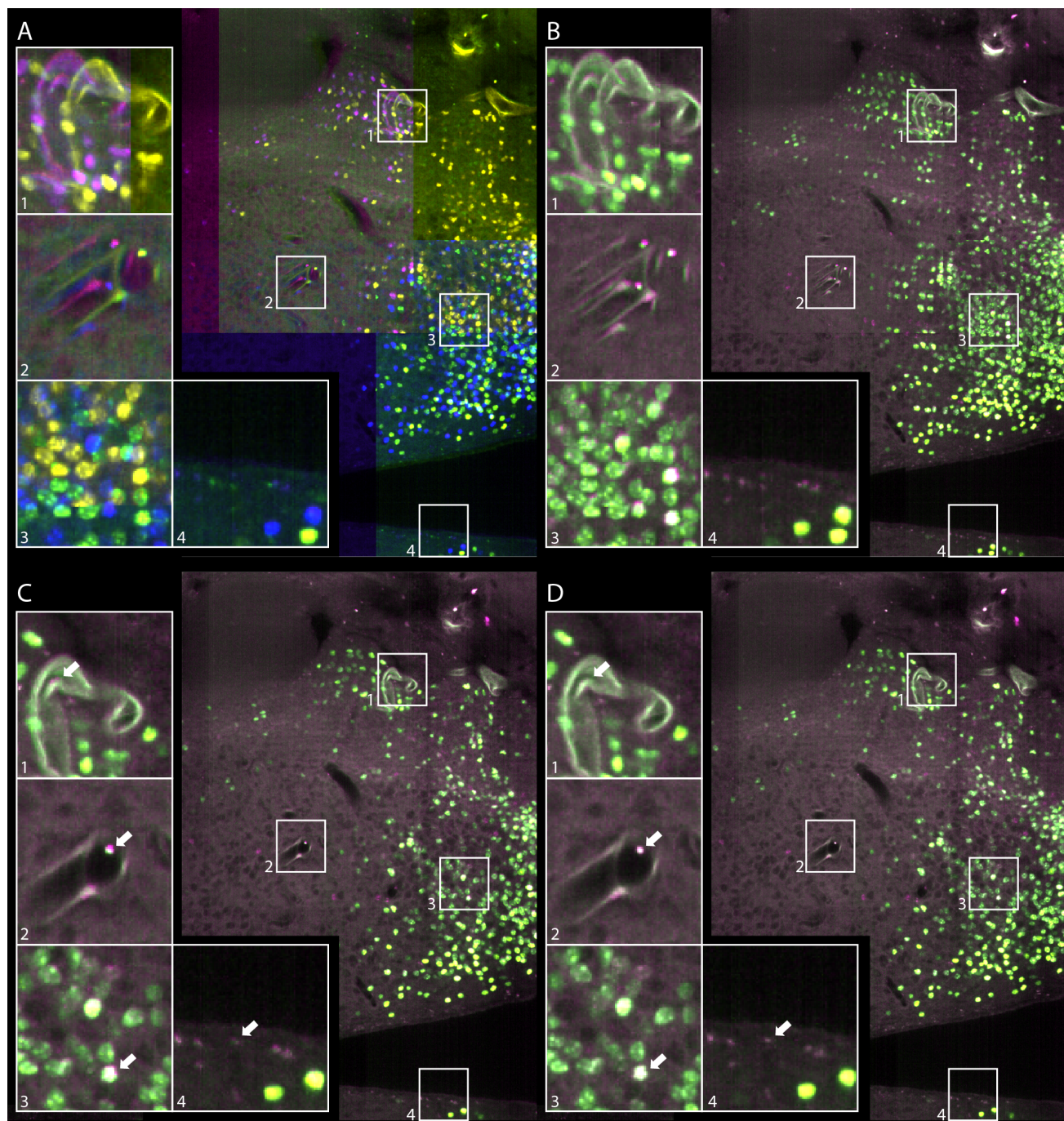
Supplementary Figure 13: *Lorem ipsum.* Dolor sit amet.

SUPPLEMENTARY FIGURE 11: Global optimization



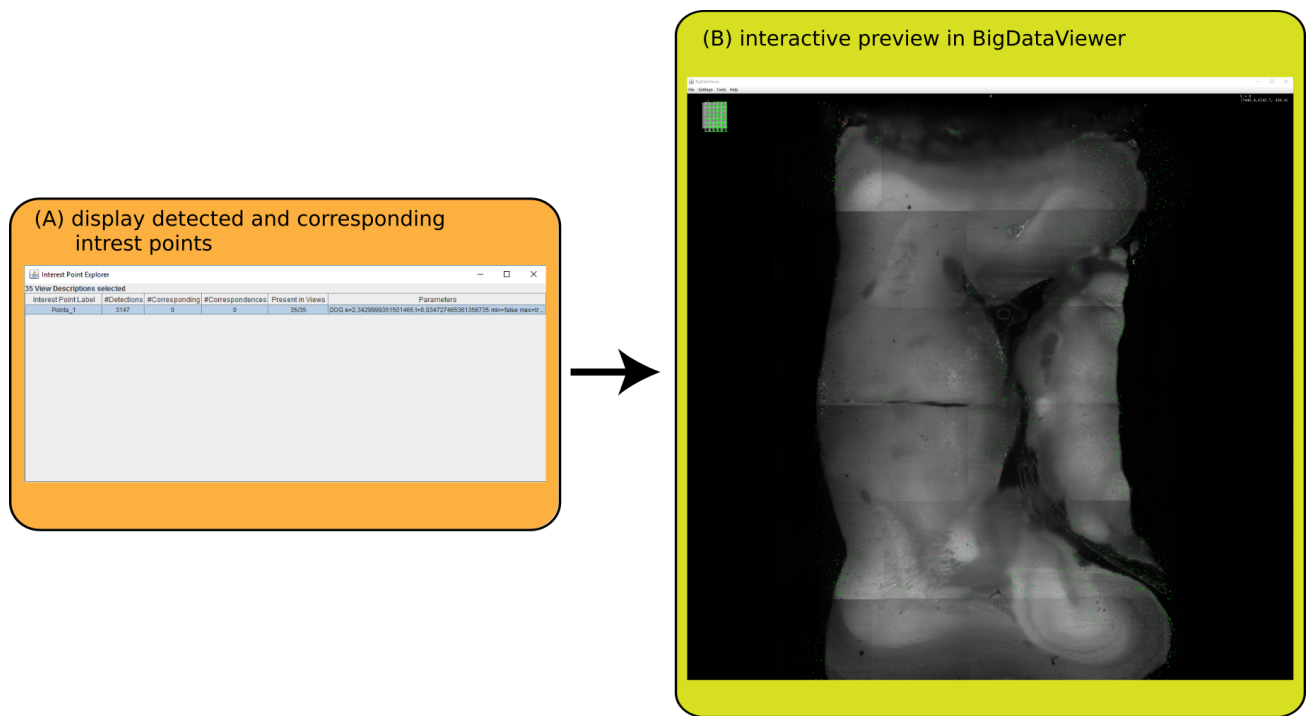
Supplementary Figure 14: *Global optimization of pairwise registration in sparse datasets.* **(A):** Simulation of a tiled image dataset with sparse objects: tiled images of multiple translated Julia fractals moved to a grid according to approximate metadata (with too high overlap). Centers of images for which pairwise shifts can be determined via phase correlation are connected by green lines, whereas centers of neighboring tiles for which no meaningful shift can be calculated are linked by dashed grey lines. Manually measured distances between distinct points in the three fractals are shown in red. Performing global optimization with *absolute shifts* (as it is done BigStitcher's predecessor, the ImageJ Stitching plugin) will correctly align images within connected components of the link graph but place all fractals close to the origin **(B)**. By using *relative shifts*, BigStitcher will leave disconnected objects at their initial location while still aligning within connected components **(C)**. As registrations are not propagated between unconnected tiles, distances between neighboring objects might change. By running a second round of optimization to align connected components according to metadata shifts and applying the results to the in-component registrations, distances between neighboring objects are preserved as-well-as-possible **(D)**.

SUPPLEMENTARY FIGURE 12: Affine refinement via ICP



Supplementary Figure 15: *Lorem ipsum. Dolor sit amet.*

SUPPLEMENTARY FIGURE 13: Interest Point visualization



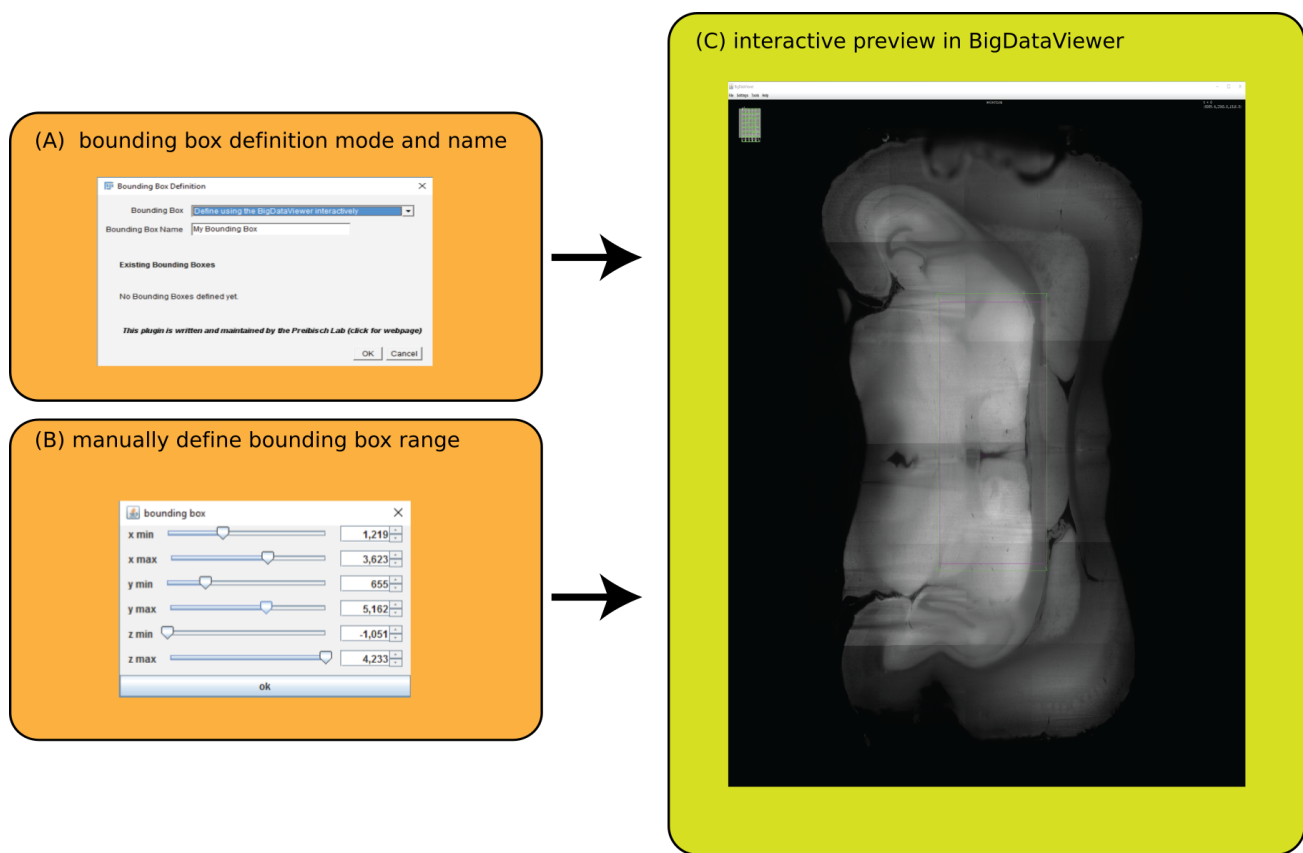
Supplementary Figure 16: *Interactive visualization of interest points.* The interest points explorer allows the visualization of interest points and corresponding interest pints between views. **(A)** select desired interest points for visualization. **(B)** preview the interest points in the BigDataViewer.

SUPPLEMENTARY FIGURE 14: Manual Transformation of multi-view datasets



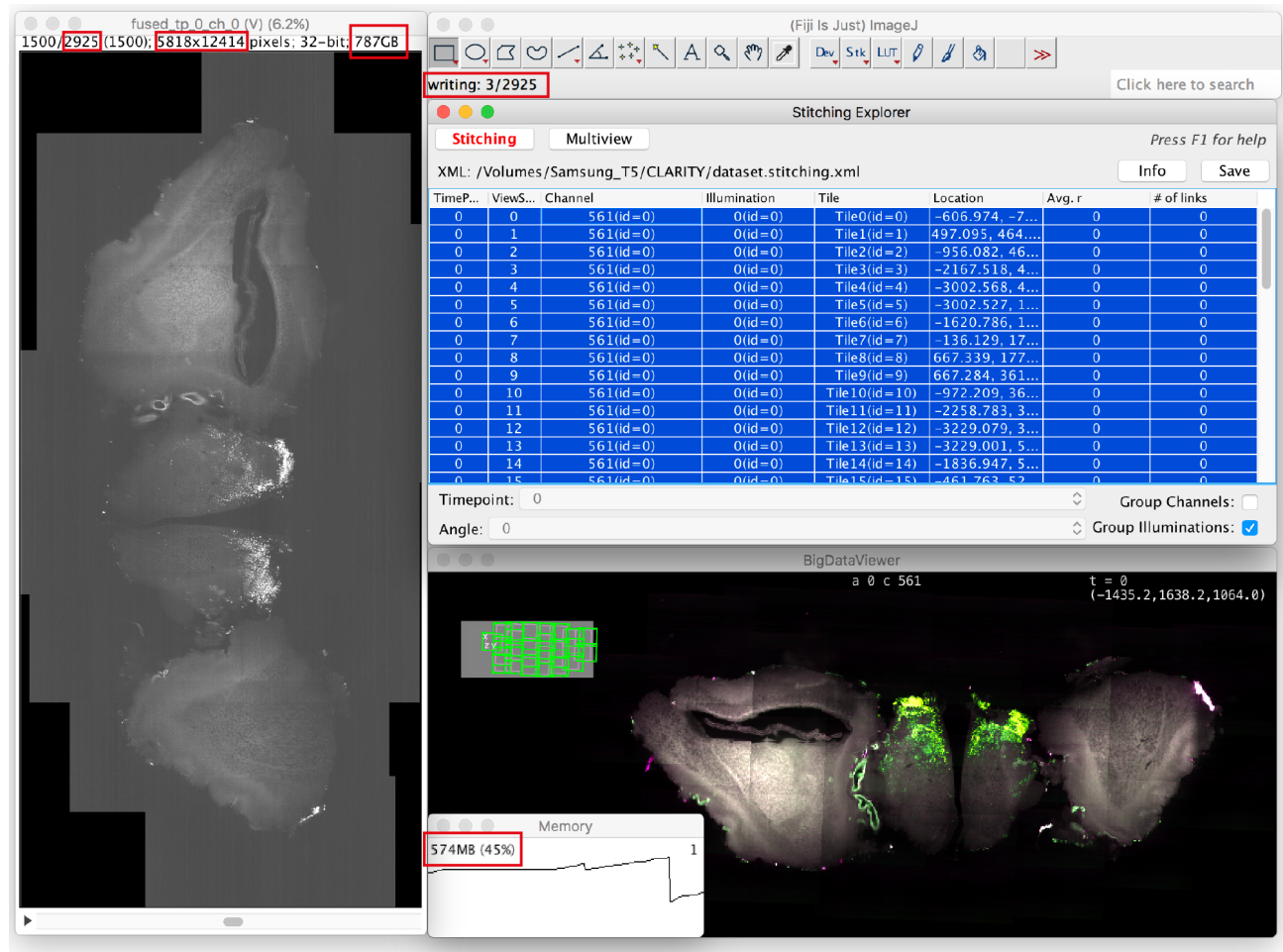
Supplementary Figure 17: *Interactive transformation of views.* Different transformation molds can be applied to one or more views and simultaneously visualized in the BigDataViewer. **(A)** Choose transformation model grouping. **(B)** Further define the transformation model. In this case a rotation around the axis is selected. **(C)** Select rotation axis and angle. **(D)** Visualize rotation of the view in the BigDataViewer.

SUPPLEMENTARY FIGURE 15: Bounding Box definition



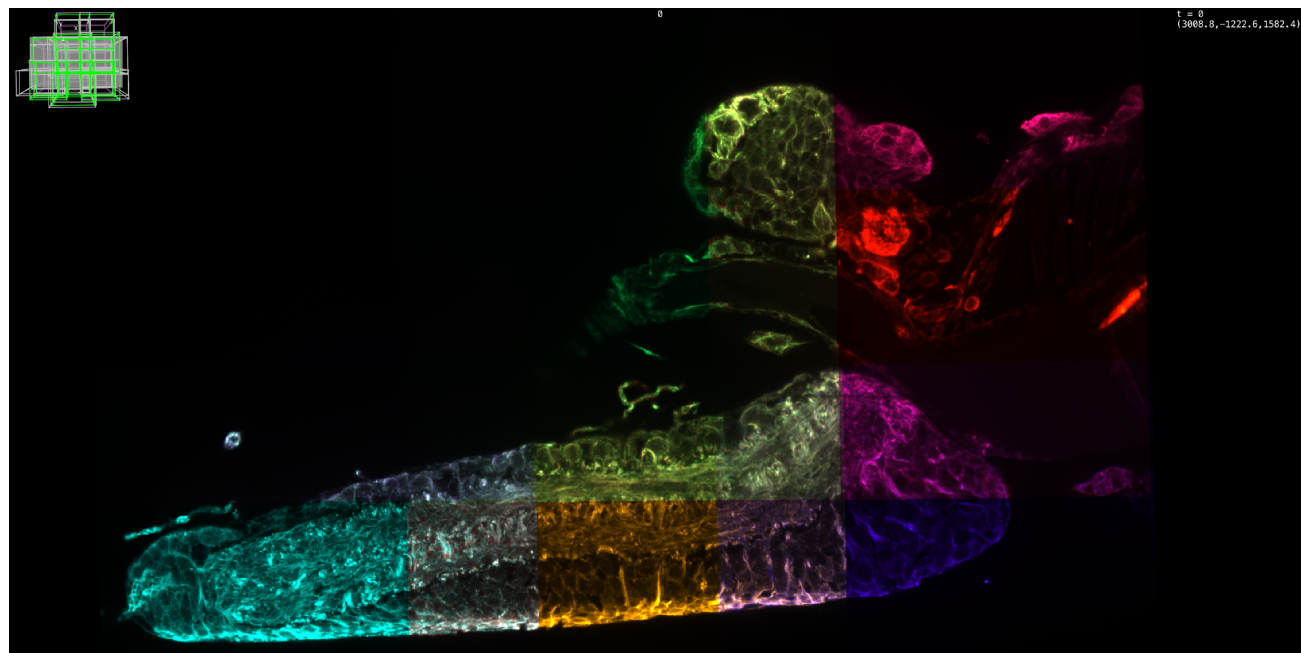
Supplementary Figure 18: *Interactive definition of bounding boxes.* The BigStitcher GUI offers the possibility of defining or modifying regions of interest via the creation of bounding boxes. **(A)** Choose the method used to define a new bounding box. In this case the interactive mode is selected. **(B)** manually define the bounding box range **(C)** Preview the size of the specified bounding box in the BigDataViewer in real-time.

SUPPLEMENTARY FIGURE 16: Virtual Fusion of large image



Supplementary Figure 19: *Lorem ipsum.* Dolor sit amet.

SUPPLEMENTARY FIGURE 13: Expansion Microscopy Stitching



Supplementary Figure 20: *Lorem ipsum.* Dolor sit amet.

SUPPLEMENTARY NOTE 1: SUPPLEMENTARY METHODS

SUPPLEMENTARY NOTE 1.1: SpimData data format

We internally represent our image data and metadata using an extended version of the SpimData data format of BigDataViewer.⁷ Each image stack is defined by a (ViewSetup, TimePoint)-combination. We extend the format by giving each ViewSetup the following *attributes*: Channel to represent color channels, Illumination to represent illumination directions, Angle to represent multi-view acquisition angles and finally Tile, representing (local) x,y points in a multipoint acquisition.

In addition to those attributes, we store detected interest points, bounding boxes (named sub-volumes in which we can *fuse* or deconvolve images), point spread functions for deconvolution and pairwise registrations (that have yet to be used in global optimization) for each (ViewSetup, TimePoint) view. For each image stack, we also store its *registration* (i.e. the transformation from pixel to world coordinates) as a list of affine transform matrices. The registration steps described below will typically prepend another transformation matrix to this list. Finally, the SpimData is associated with an ImgLoader object that can make image pixel data available as an ImgLib2 RandomAccessibleInterval given a (ViewSetup, TimePoint) *view id*.

The SpimData data structure can be saved as an XML *project file*, allowing users to manually edit it with any text editor. We automatically save previous versions of the project file to provide the user with the ability to un-do registration steps.

SUPPLEMENTARY NOTE 1.2: Import of data

BigStitcher imposes little constraints on the format and naming of raw data files. Using the Bioformats⁸ library, we support a large variety of image file formats, from "conventional" TIFF stacks to vendor-specific formats. The assignment of attributes to the image stacks in the raw data can be done automatically or with minimal interaction from the users. We offer the possibility to immediately compute multi-resolution pyramids from the images and saving them as chunks to HDF5 files. Furthermore, making use of imglib2-cache, we support virtual loading of image planes from the raw files with chaching of already loaded planes.

SUPPLEMENTARY NOTE 1.3: Flat-field correction

Flat-field correction is the process of correcting for image artifacts due to uneven illumination or detection efficiency or fixed-pattern noise. Aside from being visually unpleasing, especially in tiled acquisitions, these artifacts can also effect image registration and downstream quantitative image analyses. We therefore offer simple on-the-fly correction for a *dark image* (which might be nonzero due to e.g. camera offset) and a *bright image* (representing uneven illumination or detection efficiency across the field-of-view). We calculate corrected pixel intensities C from a raw image R and bright and dark images B and D as:

$$C_x = \frac{(R_x - D_{x'}) * \overline{(B - D)}}{(B_{x'} - D_{x'})} \quad (1)$$

The correction images can either have the same dimensionality as the raw images, in which case $x' = x$, or have lower dimensionality (e.g. when using 2D correction images on a 3D image stack), in which case $x' = (x_1 \dots x_n)$ with n being the dimensionality of the correction images. If a dark image is not provided by the user, we assume it to have constant intensity of 0 (corresponding to no background offset). Likewise, if no bright image is provided, we assume it to have constant intensity of 1 (uniform illumination and detection efficiency).

We implemented the flat-field correction as a wrapper around an ImgLoader, calculating corrected pixel intensity values on-the-fly (with optional caching) every time an image is loaded. That way, the corrected images are available for all other processing steps such as intensity-based registration, interest point detection or image fusion, but it is still possible to activate or de-activate the correction or change bright or dark images after the initial flat-field correction. A separate (bright, dark)-correction image pair can be set for every image in the dataset by modifying the XML project file, while in the GUI we offer user-friendly assignment of correction images to every (channel, illumination direction)-pair.

SUPPLEMENTARY NOTE 1.4: Pairwise shift calculation

In BigStitcher, we currently offer three ways of calculating shifts between a pair of images: the Fourier-based *phase correlation* algorithm, the Gradient-descent-based *Lucas-Kanade* algorithm, both intensity-based methods, as well as interest point-based alignment.

SUPPLEMENTARY NOTE 1.4.1: Phase correlation

By default, we calculate pairwise translational shifts using an ImgLib2 re-implementation of the Fourier-based *phase correlation* algorithm.⁷ In noiseless images, the method produces a phase correlation matrix Q containing a single δ -impulse at the location corresponding to the shift between the two images. Real images might contain multiple peaks, so we localize the n highest peaks in Q . By detecting peaks with subpixel accuracy using a quadratic fit.⁷ Aside from allowing subpixel-accurate registration, we can also use this to counteract the effects of downsampling, allowing us to perform registration of similar quality to full-resolution with significant performance gains.

Due to the periodic nature of the Fourier shift theorem, each peak in the PCM can actually correspond to 2^d possible shifts in d dimensions. We therefore test each of these candidate shifts by calculating the cross-correlation between the images with I_2 shifted according to the candidate shift (optionally with interpolation in the case of sub-pixel shifts). In the end, we keep the shift vector t corresponding the highest cross correlation as the final result (applying downsampling correction, if necessary).

SUPPLEMENTARY NOTE 1.4.2: Lucas-Kanade

In addition to the default phase correlation-based pairwise shift calculation, we offer registration via an ImgLib2 implementation of the *inverse compositional* formulation of the gradient descent-based Lucas-Kanade optical flow algorithm.⁷ While the algorithm is applicable to a variety of transformation models, we currently stick to estimating a translation vector t . If the pairwise registration converges, we calculate the cross correlation of the overlapping portions of the images as a quality metric for the pairwise registration.

SUPPLEMENTARY NOTE 1.4.3: Intensity-based Registration of grouped images

In many use cases, one might want to align not single images but groups of images, e.g. all channels of a tile, in the pairwise registration step. For this, we implemented a flexible framework for the registration of grouped images.

Each attribute of the images can be set to be an *axis of application*, an *axis of comparison* or an *axis of grouping*. The registration will proceed by first splitting the images by the application attributes, i.e. grouping all images that have the same value for these attributes. In each group, the images are then split by the comparison attributes and finally, the remaining image groups (that differ only in the grouping attributes) are combined into one image stack by either averaging all images for each grouping attribute or picking the image with a specific instance of the attribute.

In a typical application, the stitching of tiled datasets, we would, for example, start by *applying* the registration to all (Angle, TimePoint)-combinations individually, *comparing* by Tiles and finally *grouping* by Illumination and Channel for each tile, e.g. by averaging illumination directions and picking a specific channel.

SUPPLEMENTARY NOTE 1.4.4: Intensity-based registration of images with pre-registrations

The two images I_1 and I_2 can have arbitrary pre-registrations, i.e. pixel coordinates x_{px} are mapped to world coordinates x_w via the affine transforms $x_{w,I_1} = A_{I_1}x_{px,I_1} + b_{I_1}$ and $x_{w,I_2} = A_{I_2}x_{px,I_2} + b_{I_2}$. Depending on the values of A_{I_1} and A_{I_2} , we consider two cases: If they are equal, i.e. the pre-registrations differ only by a translation, we perform the shift calculation on the raw pixel data of the overlapping volume to get a shift vector t for I_2 in pixel coordinates. The transformation in world coordinates is then given by $R \begin{pmatrix} I & t \\ 0 & 1 \end{pmatrix} R^{-1}$ with $R = \begin{pmatrix} A_{I_2} & b_{I_2} \\ 0 & 1 \end{pmatrix}$. If the pre-registrations differ in more than just translation, we create virtually transformed images of the smallest rectangular bounding box enclosing the overlapping volume and use them as input to the registration. As the virtual input images are already in world coordinates in this case, the resulting transformation matrix for I_2 is simply $\begin{pmatrix} I & t \\ 0 & 1 \end{pmatrix}$.

SUPPLEMENTARY NOTE 1.4.5: Interest-point based

For interest-point based pairwise registration, we detect local extrema in either Difference-of-Gaussian or Difference-of-mean filtered images, optionally followed by subpixel refinement of the detections via a quadratic fit. If we are registering a pair of image *groups*, the interest points of each image in the group are pooled, with optional replacement of point clusters within a user-defined radius by their center.

For each image, we apply the current (affine) registrations to the pixel-coordinate interest points and then determine *candidate point matches* via descriptor matching. We then perform model-based outlier removal via the RANSAC algorithm, yielding a set of *inlier point pairs*, $C_{inliers}$, and an optimal translation t for I_2 , minimizing $\sum_{(ip_1, ip_2) \in C_{inliers}} ||ip_1 - ip_2 - t||^2$

SUPPLEMENTARY NOTE 1.5: Global optimization

SUPPLEMENTARY NOTE 1.5.1: Estimation of globally optimal transformations

The pairwise registration step results in *links* between image (groups) V (note that since we do not use the actual image *content* in the global optimization, we will refer to the images by their integer *id* in this section: $V \subset \mathbb{N}$). The links can be either in the form of pairwise transformations T^p (such that coordinates x from two images V_i and V_j can be transformed according to $T_{ij}^p(x_j) = x_i$) or *point correspondences* PM from which such transformations can be estimated. The pairwise registrations thus form a *link graph* (V, C) with edges $C = \{(i, j) \in V \times V | T_{ij}^p \in T^p\}$ between image pairs for which we could determine pairwise transformations. Simply traversing a spanning tree of the link graph and propagating the pairwise transformations can lead to the compounding of pairwise registration errors, even if the traversal is done along a *minimal* spanning tree determined according to some quality metric q_{ij} , e.g. cross-correlation, of the pairwise registrations.

We thus make use of an algorithm for globally optimal registration by iterative minimization of square displacement of point correspondences² for reaching a reasonable consensus in this case. This point match-based framework allows for flexible grouping and fixing of images, is applicable to, among others, time series-, chromatic channel- or view-registration and can easily be adapted to incorporate the pairwise transformations from e.g. phase correlation. The algorithm is agnostic of the transformation model (e.g. translation, affine transform,...), with the only requirement being that the model parameters can be estimated by a least-squares fit from point correspondences.

We determine the globally optimal registrations R given the image (groups) V , pairwise links C , pairwise n -dimensional point matches PM with $PM_{ij} \subset \mathbb{R}^n \times \mathbb{R}^n$ and a set of fixed views $F \subseteq V$ by minimizing:

$$\arg \min_{R \setminus \{R_i | V_i \in F\}} \sum_{(i, j) \in C} \left(\sum_{(x_k, y_k) \in PM_{ij}} \|R_i(x_k) - R_j(y_k)\|^2 \right) \quad (2)$$

Note that for all fixed views, the registration will be constrained to be the identity transformation I : $\forall V_i \in F : R_i = I$.

SUPPLEMENTARY NOTE 1.5.2: Global optimization given pairwise transformations

The intensity-based pairwise shift calculations do not directly give us the point correspondences we need for the global optimization step, instead the results are pairwise transformations T^p in the form of affine transform matrices. We can, however, easily construct point correspondences by taking a set of points and transforming them with the *inverse* transform (the only requirement being that the n -dimensional points do not all lie in a subspace of lower dimensionality of \mathbb{R}^n).

Using the 3-dimensional pairwise transformations T^p ($T_{ij}^p(x_j) = x_i$) between two image (groups) V_i and V_j given their existing registrations R^{meta} , we use the 8-point approximate bounding box of their overlapping region BB_{ij} to construct the point correspondences: $PM_{ij} = \{(bb_k, (T_{ij}^p)^{-1}(bb_k)) | bb_k \in BB_{ij}\}$. We can then determine the globally optimal registrations R by performing the minimization described above (2).

SUPPLEMENTARY NOTE 1.5.3: Global optimization with iterative link dropping

Once the global optimization terminates due to convergence or exceeding of the maximum number of iterations, we can calculate the *error* of the individual images as the average displacement of all interest points in an image to their point matches:

$$e_i = \frac{\sum_{\{j:(i,j) \in C\}} \sum_{(x_k, y_k) \in PM_{ij}} \|R_i(x_k) - R_j(y_k)\|}{\sum_{\{j:(i,j) \in C\}} |PM_{ij}|} \quad (3)$$

If the link graph (V, C^n) contains links with contradicting point correspondences, stopping after one round of global optimization might leave us with unsatisfying results. In the *iterative* version of the global optimization, we therefore check that both the average error of all images and the ratio of maximal and average error fall below a user-defined threshold. If these conditions are not yet met, we will proceed to iteratively remove disagreeing links from the link graph and repeat the global optimization. To do this, we first determine the link with the highest error by maximizing:

$$c_{worst} = \arg \max_{(i,j)} \max_{(x_k, y_k) \in PM_{ij}} \left((1 - q_{ij})^2 \sqrt{d_{ijk}} \log_{10} \left(\max(\deg(i), \deg(j)) \right) \right) \quad (4)$$

with d_{ijk} denoting the distance of the k 'th point match of the link (i, j) , $d_{ijk} = \|R_i(x_k) - R_j(y_k)\|$, $\deg(i)$ denoting the degree (number of neighbors) of an image V_i in the link graph and q_{ij} being a *quality metric* $\in (0, 1)$ of the link, e.g. 0-truncated cross correlation. We then remove the worst link from the links ($C^{n+1} \leftarrow C^n \setminus c_{worst}$) and repeat the optimization step 2 with the new link graph (V, C^{n+1}) . The whole process is repeated until the errors fall below a user-defined threshold (in the worst case, links will be dropped until we end up with *spanning trees* of the connected components in the link graph).

SUPPLEMENTARY NOTE 1.5.4: Two-round global optimization using metadata

If some cases, the link graph might contain multiple connected components, e.g. in datasets from screening applications, where the actual sample only occupies isolated "islands" and most images contain only background. In this case, we can only reliably determine pairwise transformations within the connected components and align images within the components in the global optimization step. We might, however, have reasonable registrations R^{meta} from metadata and wish to keep as closely as possible to those if we do not have *strong* links.

For this, we offer a *two-round* version of the global optimization. In the first round, we determine registrations R^{strong} as described above, using the graph of *strong* links, i.e. links that are backed by pairwise transformations. In the second round, we determine the connected components in the (V, C^{strong}) graph and a mapping $CC : \mathbb{N} \rightarrow \mathbb{N}$ from image (group) indices to connected component indices as well as *weak links* $C^{weak} = \{(i, j) \in V \times V \mid CC(i) \neq CC(j)\}$ between images in different components. We then determine transformations R^{cc} for each connected component not containing a fixed image by minimizing:

$$\arg \min_{R^{cc} \setminus \{r_i^{cc} \in R^{cc} \mid CC_i \cap F \neq \emptyset\}} \sum_{(i,j) \in C^{weak}} \sum_{bb_k \in BB_{ij}} \|R_{CC(i)}^{cc}(R_i^{strong}(bb_k)) - R_{CC(j)}^{cc}(R_j^{strong}(bb_k))\|^2 \quad (5)$$

Note that we use the corners bb_k of the bounding box BB_{ij} of the overlapping volume of two images V_i and V_j as the point correspondences. The overlap is determined according to the metadata transformations R^{meta} and we essentially try to "un-do" the registrations of the first round as well as possible (while keeping the registrations *within* the connected components). The final transformations R are the concatenation of the registrations within the connected components with the relative transformations of the connected components: $R_i \leftarrow R_{CC(i)}^{cc} R_i^{strong}$.

SUPPLEMENTARY NOTE 1.6: MultiView Registration

For MultiView registration, e.g. registration of angles or time series stabilization, we first detect interest points in the individual images as described above (1.4.5). Images may be grouped (and are by default if we are, e.g. registering tiled acquisitions from multiple angles for which we already aligned the tiles via an intensity-based method) according to their attributes, by pooling their interest points and optionally merging clusters. For registering time-series data, we offer four strategies. First, we can treat time points individually, registering only images within a time point. We can also perform interest point matching between different time points, either comparing all-to-all, all to a user-defined *reference* time point or all time points within a defined range to each other.

Pairwise point correspondences can either be established by descriptor matching followed by RANSAC outlier removal, a modified version of the iterative closest point (ICP) algorithm or by simply matching the center of mass of the point clouds of both images (note that in this case the registration will be constrained to be a translation). Using the link graph (V, C) and pairwise point correspondences P_{ij} established thus, we calculate the final registration by performing global optimization as described above (1.5), optionally with iterative link removal and a second round to preserve metadata.

SUPPLEMENTARY NOTE 1.7: Image Fusion

We *fuse* multiple images by performing a weighted average of the raw images I^{raw} transformed by their registrations R . Each raw image I_i^{raw} has a set weight images W_i . For example, we allow the user to weigh the images with a cosine-shaped fade-out, deemphasizing the artifact-prone border regions of the individual images, as well as by the approximate local entropy, to emphasize images with sharper structures in overlapping regions. Since the raw images will be evaluated at non-integer coordinates, we offer the choice between nearest-neighbour and linear interpolation. Downsampling can easily be achieved by prepending a scaling transformation to each of the registrations R . The intensity of the fused volume at a coordinate x is given by:

$$I^{fused}(x) = \frac{\sum_{I_i^{raw} \in I^{raw}} \left(I_i^{raw}(R_i^{-1}(x)) * \prod_{w_j \in W_i} w_j(R_i^{-1}(x)) \right)}{\sum_{I_i^{raw} \in I^{raw}} \left(\prod_{w_j \in W_i} w_j(R_i^{-1}(x)) \right)} \quad (6)$$

In practice, we evaluate I^{fused} only at integer coordinates of a user-defined *bounding box*. We implemented the image fusion to perform all calculations virtually on-the-fly, with caching of previously computed planes using imglib2-cache. This allows the quick inspection of fusion results as well as creation and planewise saving of images that might exceed the RAM available to the user.

SUPPLEMENTARY NOTE 2: BIGSTITCHER USER GUIDE

The BigStitcher comes with extensive documentation that is hosted on the ImageJ wiki. The current version of the continuously updated user guide can be found at <https://imagej.net/BigStitcher#Documentation>.

SUPPLEMENTARY NOTE 3: LINKS TO THE CURRENT SOURCE CODES

BigStitcher can be seen as an extension to the multiview-reconstruction project, but over time, many changes have been pushed upstream and the two projects have evolved in parallel. Both projects are licensed under the GPL(v2) and the source code is freely available on GitHub, at <https://github.com/PreibischLab/BigStitcher> and <https://github.com/PreibischLab/multiview-reconstruction>, respectively.

The CUDA code for accelerated interest point detection and devonvolution is available from <https://github.com/StephanPreibisch/SeparableConvolutionCUDALib> and <https://github.com/StephanPreibisch/FourierConvolutionCUDALib>, respectively.

Newer versions will be hosted using GitHub, and release announcements will be done on the GitHub page (<https://github.com/PreibischLab/BigStitcher>) and on the ImageJ wiki (<http://imagej.net/BigStitcher>). Releases are and will be provided to end users via the Fiji update mechanism. The current version of the user guide (2) will be hosted on the same wiki page (<http://imagej.net/BigStitcher#Documentation>).